NUCL SCI TECH (2020) 31:48
https://doi.org/10.1007/s41365-020-00755-0

Compact 16-channel integrated charge-sensitive preamplifier module for silicon strip detectors

Dong-Xi Wang[1] · Cheng-Jian Lin[1] · Lei Yang[1] · Nan-Ru Ma[1] · Li-Jie Sun[1] · Feng Yang[1] · Hui-Ming Jia[1] · Fu-Peng Zhong[1] · Pei-Wei Wen[1]

Received: 22 January 2020 / Revised: 21 February 2020 / Accepted: 21 February 2020 / Published online: 4 May 2020

Abstract In this study, a compact 16-channel integrated charge-sensitive preamplifier named the smart preamplifier (SPA) was developed to support the large-scale detector array used in modern nuclear physics experiments. Two types of SPA, namely SPA02 and SPA03 (with external field effect transistor), have been manufactured to match silicon detectors with small and large capacitances, respectively. The characteristics of the SPA include fast response of typically less than 6 ns for pulse rising time and low equivalent noise of 1.5 keV at zero input capacitance. The energy sensitivity and pulse decay time can be easily adjusted by changing the feedback capacitance C_f and resistance R_f in various applications. A good energy resolution of 24.4 keV for 5.803-MeV alpha particles from ^{244}Cm was achieved using a small-sized Si-PIN detector; for the silicon strip detectors in the test with the alpha source, a typical energy resolution of 0.6–0.8% was achieved. The integrated SPA has been employed in several experiments of silicon strip detectors with hundreds of channels, and a good performance has been realized.

Keywords Silicon strip detector array · 16-Channel integrated charge-sensitive preamplifier · Preamplifier circuit design · Preamplifier performance

1 Introduction

With the development and application of the radioactive ion beam (RIB), new physical phenomena have been revealed in exotic nuclei which are distant from the β-stability line, such as the halo or skin structures [1, 2] and the new magic numbers [3]. To overcome the low intensity and quality of the RIB, the detection efficiency has been improved experimentally by using a large solid angle covered detector array. The silicon detectors, especially the single- or double-sided silicon strip detectors (SSSDs or DSSDs) with efficient energy and spatial resolutions for charged particles, have been widely applied in building silicon detector arrays with a large and continuous angular coverage. A number of silicon detector arrays, such as MUST [4, 5], GLORIA [6], TIARA [7], EXODET [8], EXPADES [9], and MITA [10], have been developed for experimental studies motivated from the RIB.

A preamplifier is a key electronic module for realizing impedance matching between the detector and spectroscopy amplifier; it plays an important role in reducing external interference and consequently improving the signal-to-noise ratio. The ORTEC charge-sensitive preamplifier modules 142A, 142B, and 142C [11] that feature low noise and fast rising time (T_{rise}) were designed mainly for the optimal matching of each individual charged-particle detector. However, processing the hundreds of signals produced by the silicon detector array is challenging for the traditional discrete preamplifier modules. Consequently,

This work was supported by the National Key R&D Program of China (No. 2018YFA0404404), the National Natural Science Foundation of China (Nos. 11635015, U1732145, 11705285, 11805280, U1867212, and 11961131012), and the Continuous Basic Scientific Research Project (No. WDJC-2019-13).

✉ Cheng-Jian Lin
cjlin@ciae.ac.cn

1 Department of Nuclear Physics, China Institute of Atomic Energy, Beijing 102413, China

specially designed electronic systems are required to support these complex detector arrays. The integrated Mesytec MPR-16 module [12] provides 16-channel preamplifiers specially designed for SSSD or DSSD. However, owing to its large size, it is difficult to install it close to the detectors in a limited chamber space. To reduce the crosstalk and noise, a special preamplifier module that is not commercialized to match other silicon detector arrays has been designed for MUST [4, 5]. Preamplifiers based on the application-specific integrated circuit (ASIC), such as VATA from IDEAS [13–15], were used for the silicon detectors. The IDEAS integrated circuits, however, are available only as bare dice or packaged chips, making it difficult for VATA to match the existing amplifier modules and data acquisition systems.

For the individual readout of each strip of the large-scale silicon detector array, the application of the highly integrated and low-cost preamplifier modules is definitely required. Therefore, a compact 16-channel integrated charge-sensitive preamplifier named the smart preamplifier (SPA), based on the commercial integrated circuit operational amplifier (OPA), has been designed and manufactured. With the compact size feature, the SPA can be placed in a vacuum chamber with water cooling and directly connected to the silicon detectors to significantly reduce noise. The performance was tested by using the alpha sources and further confirmed by the in-beam experiments performed using both the HI-13 tandem accelerator of the China Institute of Atomic Energy (CIAE) and the Radioactive Ion Beam Line in Lanzhou (RIBLL1) of the Institute of Modern Physics (IMP), Chinese Academy of Sciences.

2 Circuit design for the preamplifier

The SPA circuit mainly consists of three core parts: the bias circuits composed of R_1, R_2, and C_1, the input part composed of input and test capacitors C_0 and C_2, and the amplification-stage circuit composed of an OPA and resistor–capacitor feedback network R_fC_f.

A simplified block diagram of the SPA02 is shown in Fig. 1a. The bias voltage for the detector is supplied via the bias resistor R_2. To reduce the noise coming from the high-voltage cable, the first-order RC filter circuit consisting R_1 and C_1 was employed. The maximum high voltage can reach 500 V, which is enough for most silicon detectors. C_0 is a coupling capacitor which couples the detector signal to the input end of the OPA and isolates the direct current (DC) to guarantee a stable quiescent point for the post-stage circuit. The function of C_2 is the same as that of C_0 but for the test signal. The PA labeled in Fig. 1 is a high-

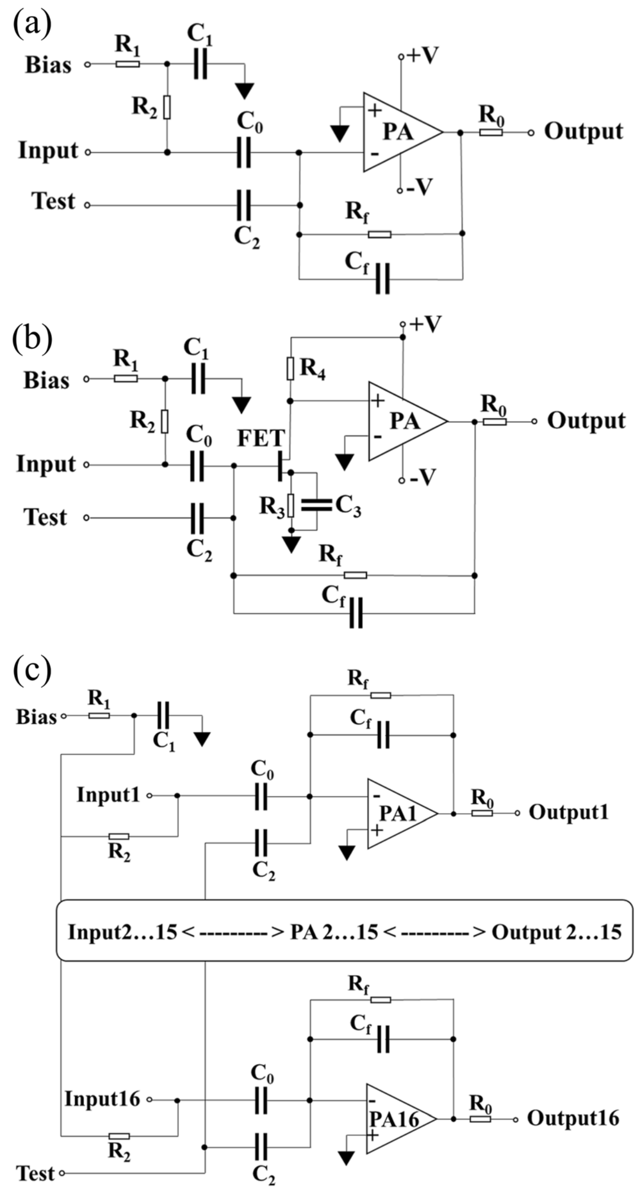

Fig. 1 Simplified block diagrams of SPA02 (**a**), SPA03 (**b**), and SPA02-16 (**c**)

performance commercial integrated circuit OPA. OPA657 [16] manufactured by Texas Instruments was applied, which is characteristic of a low input voltage noise of 4.8 nV/$\sqrt{\text{Hz}}$, high gain bandwidth of 1.6 GHz, and DC precision of a trimmed junction field effect transistor (JFET) input stage to give an exceptionally high input impedance. The R_0 series resistor at the output terminal provides a matching load for the subsequent equipment. The resistor–capacitor feedback network R_fC_f forms a charge integrating and bleeding circuit that determines the energy sensitivity and pulse decay time. The energy sensitivity can be easily changed on request. The performance of SPA02 for the low capacitance silicon detectors is efficient and will be discussed later.

To match the high capacitance (approximately 1000 pF) SSSD or DSSD, such as a SSSD with a thickness of 20 μm (W1-type from Micron Semiconductor Ltd. [17]), it is necessary to ensure that the dynamic input capacitance of the preamplifier, which depends on the corresponding transconductance, is considerably larger than the detector capacitance. To address this requirement, another preamplifier type, named the SPA03 was developed, as shown in Fig. 1b. For the amplifier to have a sufficiently high transconductance, the commercial JFET BF862 [18] from Philips Semiconductors with the advantages of a high transition frequency (640 MHz) and a high transconductance ($g_{\mathrm{m}} = 40\,\mathrm{mS}$) was used in the first amplification stage. A common source circuit of the field effect transistor (FET) employed in the first stage features a high input impedance, low noise, and wide bandwidth. The gain value of the FET connected with the common source circuit is $A_1 = -g_{\mathrm{m}} R_4 = -40\ \mathrm{mS} \times 680\ \Omega = -27.2$. Because of the high gain in the first stage, the capacitance reflected to the input from the drain to gate capacitance will be significant [19] owing to the Miller effect. The high transconductance reduces the series noise contribution, which is the most significant factor to receive a good output signal for a high-capacitance detector. The current feedback OPA AD8001 [20] developed by Analog Devices was used as the second amplification stage to meet the requirement of a fast response and low power consumption. The AD8001 features a low power consumption of 50 mW, a wide bandwidth of 800 MHz, and a slew rate of 1200 V/μs.

Eight SPA02s were installed to a ceramic circuit substrate with a size of 24 mm × 80 mm to easily match the silicon detector array with hundreds of channels. This unit shown in Fig. 2a was named the SPA02-08. Further, to match both the strip detector with 16 strips and the main amplifier module with 16 channels, the SPA02-16 (Fig. 1c) was assembled using two pieces of SPA02-08 positioned back-to-back, as shown in Fig. 2c. The Rogers ceramic printed circuit board (PCB) was adopted to provide efficient heat conduction. Standard 2.54-mm pin connections were employed for the input and output signals as well as the common input of the ± 6 V power supply, bias, and test signals. SPA03-08 (Fig. 2b) and SPA03-16 can be assembled similarly. With this compact design, the silicon detectors can be connected to the SPAs using short cables in actual use for improving the signal quality.

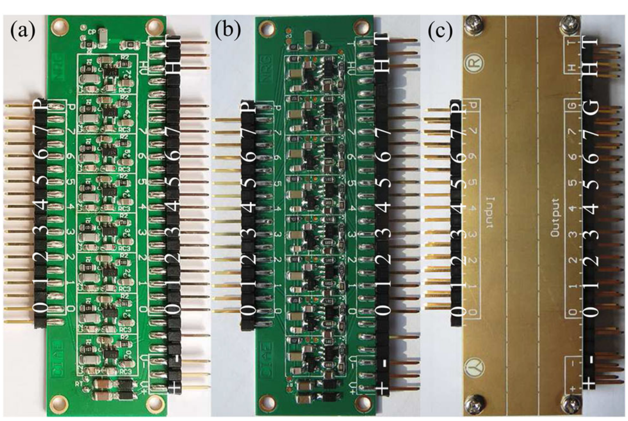

Fig. 2 (Color online) Photographs of SPA02-08 (**a**), SPA03-08 (**b**), and PA02-16 (**c**). "±" is the power supply of 6 V, "H" represents the bias for the detector with a 100-MΩ protection resistor, "T" denotes the test pulse input, protection is represented by "P", and "G" and other areas without labels are the earthed regions

3 Performance test for the preamplifier

We tested the SPAs in detail using a pulse generator and alpha source, to have a better understanding of the performance of the preamplifiers. Both the positive and negative input signals are acceptable for SPA02 and SPA03. The baseline drift of the output signal is typically less than ± 20 mV and at most ± 50 mV over the full output range of ± 2 V with a 50 Ω terminal. Based on the test results, the SPAs were further applied in the in-beam experiments and showed good quality and high stability.

3.1 Response linearity

An exponential attenuation signal with an adjustable pulse amplitude of 0–1300 mV and frequency of 1 kHz, supplied by the precise pulse generator AFG3022C manufactured by Tektronix [21], was used for the linearity test. The output amplitude (V_{out}) was obtained by the CAEN N1568A [22] spectroscopy amplifier and CAEN V785 [23] peak-sensing analog-to-digital conversion (ADC). Figure 3 shows the result of the linearity test; good linearities are observed for both SPA02 and SPA03 with determination coefficients of $R^2 = 0.99953$ and $R^2 = 0.99990$, respectively.

3.2 Influence of input capacitance

An exponential attenuation test signal with 1 kHz and 800 mV was fed to SPA02 and SPA03 with $R_{\mathrm{f}} = 100\ \mathrm{M}\Omega$ and $C_{\mathrm{f}} = 1\ \mathrm{pF}$, respectively. The amplitude and rising time of the output signal were obtained using an oscilloscope DPO 4034B manufactured by Tektronix [24] with a 50 Ω terminal. Equivalent noise was extracted by fitting the output spectrum acquired by N1568A [22] and V785 [23]. To clearly demonstrate the performance of the SPA and

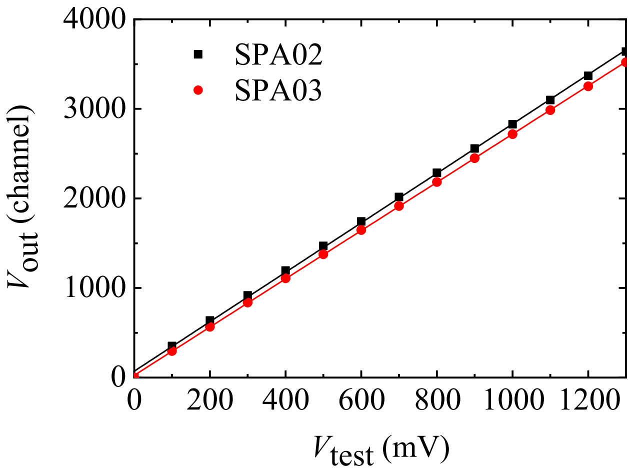

Fig. 3 (Color online) Linearity test between V_{out} and V_{test} for SPA02 and SPA03

compare with that of the preamplifiers manufactured by ORTEC and Mesytec, the equivalent noise was calibrated using the ^{239}Pu and ^{241}Am alpha sources and keV was used as the physical unit when quoting the equivalent noise of the preamplifiers.

The dependences of V_{out}, T_{rise}, and equivalent noise (Noise) on the input capacitance (C_{in}) are shown in Fig. 4. It can be seen from Fig. 4a that the V_{out} of SPA03 changes gradually compared with that of SPA02 with the increase in C_{in}. Figure 4b shows that the T_{rise} of SPA02 and SPA03 increases with the increase in C_{in}. Both SPA02 and SPA03 have a fixed rising time of generally less than 6 ns at $C_{in} = 0\,\text{pF}$ within the full output range. The "Noise Slope," defined as the variation of the equivalent noise with C_{in}, is shown in Fig. 4c. The equivalent noises of both SPA02 and SPA03 are less than 1.5 keV without external C_{in}. The equivalent noise of SPA03 is lower than that of SPA02, especially at large C_{in}, as shown in Fig. 4c. The parasitic capacitance of a silicon strip with an area of 3 mm × 50 mm for a SSSD with a thickness of 20 μm is approximately 1000 pF. Therefore, SPA03 is more suitable for high-capacitance detectors. The relevant parameters of the rising time, equivalent noise, and noise slope for SPA02 and SPA03 along with the 142A/B/C and MPR-16 are listed in Table 1.

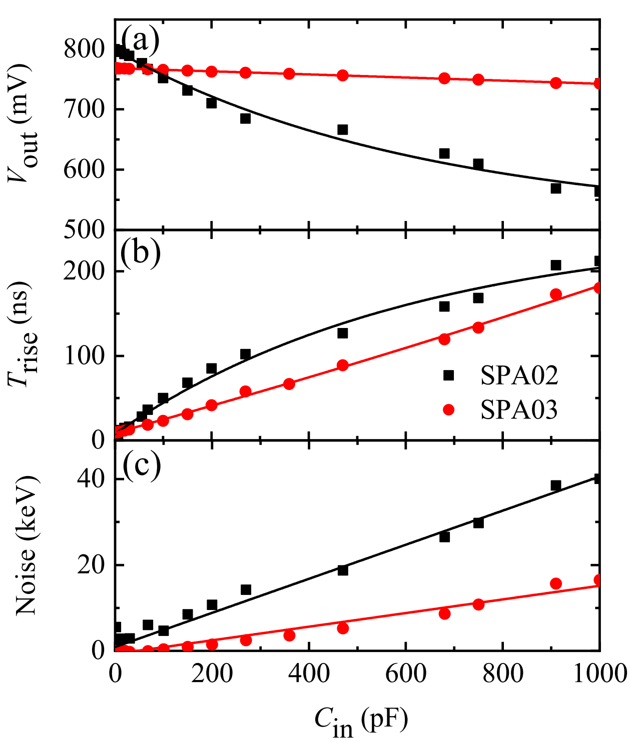

Fig. 4 (Color online) Variations of the output amplitude (V_{out}), rising time (T_{rise}), and equivalent noise (Noise) with the external input capacitance (C_{in}) for SPA02 and SPA03 with $R_f = 100\ \text{M}\Omega$ and $C_f = 1\,\text{pF}$ for the input pulse high $V_{in} = 800\,\text{mV}$

3.3 Energy resolution and energy dynamic range

A triple mixed alpha source composed of ^{239}Pu, ^{241}Am, and ^{244}Cm was used to evaluate the energy resolution of the Si-PIN detector with an effective area of 5 mm×5 mm ($C_{det} \approx 9\,\text{pF}$) equipped with the SPA02. A typical energy spectrum is shown in Fig. 5. The types of alpha sources, energies, and energy resolutions are marked. An energy resolution of 0.42% was obtained for 5.803 MeV alpha particles from ^{244}Cm by fitting the main peak. For a cooperative production of the DSSD manufactured by CIAE and the Beijing Kelixing Photoelectric Technology [25], with an active area of 48 mm × 48 mm and a thickness of 300 μm, the energy resolutions for a triple mixed alpha source have been achieved at 0.65–0.80% for the junction strips and 0.85–1.00% for the ohmic strips of the DSSD equipped with the SPA02.

A ^{239}Pu alpha source was used to measure the energy resolution of a SSSD with a thickness of 300 μm equipped with SPA02-16 or SPA03-16 modules. The connection between the SSSD and SPA-16 is shown in Fig. 6a. The

Table 1 Performance of SPA02, SPA03, 142A/B/C, and MPR-16

Preamplifier type	T_{rise}^{a} (ns)	Equivalent noise[a] (keV)	Noise slope (eV/pF)
SPA02	6	1.5	397
SPA03	6	1.5	159
142A	5	1.6	180
142B	5	1.4	176
142C	5	2.2	124
MPR-16	12	4.0	400

[a] These values are obtained under $C_{in} = 0\,\text{pF}$

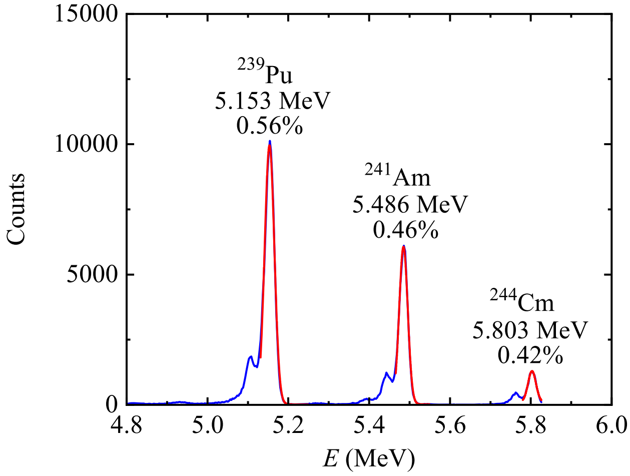

Fig. 5 (Color online) Energy spectrum of the alpha particles from the triple mixed source measured by a Si-PIN detector with SPA02

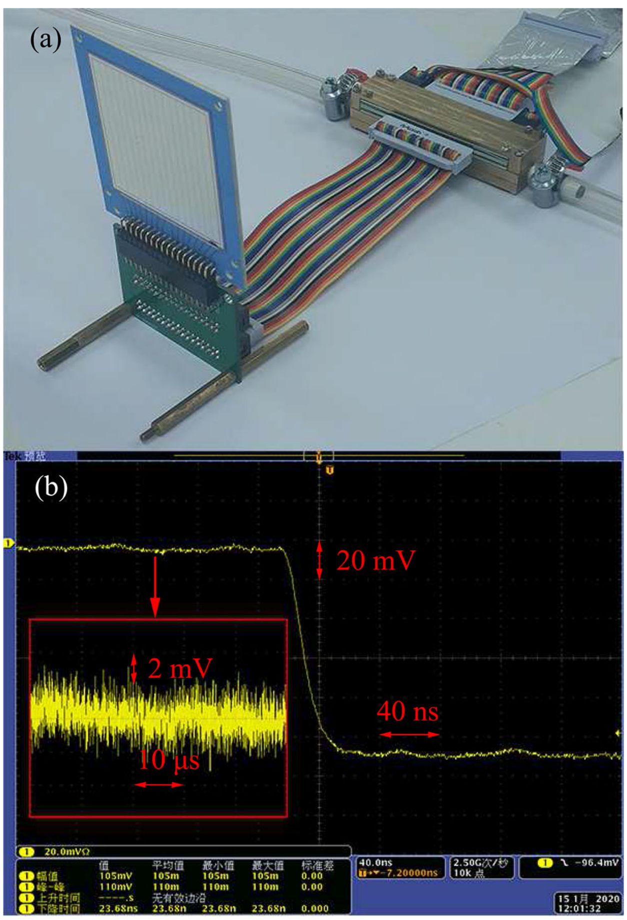

Fig. 6 (Color online) **a** Photographs of SSSD of thickness 300 µm with an SPA02-16 module and cooling plate. **b** Pulse shape and noise of the 5.153 MeV alpha particles measured by the SSSD equipped with SPA02-16 ($R_f = 100$ MΩ and $C_f = 1$ pF)

alpha source was placed at a distance of 10 cm from the SSSD with an effective area of 50 mm × 50 mm. The output pulse shape and noise of the SPA02-16 module with $R_f = 100$ MΩ and $C_f = 1$ pF for the 5.153 MeV alpha particle detected by the SSSD with a thickness of 300 µm and a bias of − 50 V are shown in Fig. 6b. The pulse shape for the 5.153-MeV alpha particle features T_{rise} of 24 ns, output amplitude of 105 mV, and noise amplitude of 2 mV with a 50 Ω terminal. The output of SPA02 or SPA03 was fed directly to N1568A [22] and then to V785 [23].

To achieve better energy resolution and to maintain operational stability, the SPA modules were cooled to about 10°C using a circulating cooling machine. Figure 7 shows the measured α-energy spectra using SPA02 (a) and SPA03 (b), respectively. The obtained energy resolutions are 0.73% and 0.67% for SPA02 and SPA03, respectively. The small bumps at 5.499 MeV originate from contamination with ^{238}Pu.

The energy dynamic range (EDR) was extracted using the output amplitude of the 5.486-MeV alpha particle (α-amp) from ^{241}Am in the Si-PIN with SPA02 or SPA03 by varying C_f. The C_f of SPA02, corresponding energy sensitivity, EDR, and the output amplitude are listed in Table 2. The energy sensitivity of SPA03 is almost identical to that of SPA02 and is not shown here. Compared

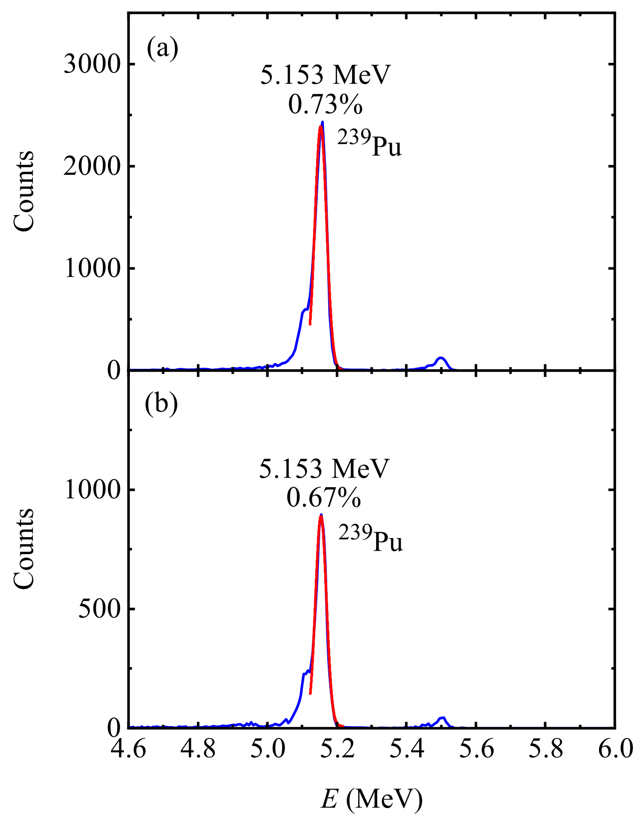

Fig. 7 (Color online) α energy spectra measured by the SSSD with SPA02 (**a**) and SPA03 (**b**)

Table 2 Relation of the output amplitude of the alpha particles (α-amp), energy dynamic range, and energy sensitivity with C_f for SPA02

C_f (pF)	α-amp[a] (mV)	EDR (MeV)	Sensitivity (mV/MeV)
1	108	100	20.0
2	60	183	10.9
3	38	289	6.9
4	28	392	5.1
5	25	439	4.6

[a] α-amp was obtained using the oscilloscope DPO 4034B with a 50 Ω terminal

with the fixed EDR for the preamplifiers made by both ORTEC and Mesytec, the EDR of the current SPA can be easily changed by modifying C_f to match the different requirements.

3.4 Application to in-beam experiments

The integrated SPA modules were applied to in-beam experiments performed at the HI-13 tandem accelerator of CIAE [26–28]. To study the one-proton transfer reaction of $^{7}Li+^{208}Pb$, a detector array containing 16 Si-PIN detectors, four multi-layer ionization-chamber (IC) telescopes [10], and two silicon detector telescopes was used. The multi-layer IC telescope consists of one IC, one 60-μm-thick DSSD (W1-type from Micron Semiconductor Ltd. [17]), and two quadrant silicon detectors (QSDs) with thicknesses of 300 μm and 1000 μm, respectively. The silicon detector telescope includes one 20-μm-thick SSSD, one 60-μm-thick DSSD, and one-1000-μm-thick QSD. Therefore, two SPA03-16 and seventeen SPA02-16 modules were applied for the two 20-μm-thick SSSDs and other detectors, respectively.

The photograph of the assembled detector array with the SPA modules and cooling copper ring is shown in Fig. 8a. Figure 8b represents a typical ΔE-E_R spectrum obtained by the silicon detector telescope located at $\theta_{lab} = 144° - 171°$ at $E_{lab} = 28.55$ MeV. The corresponding kinetic energy spectrum of ^{6}He is shown in Fig. 8c. The excitation energies of ^{209}Bi can be calculated using the kinetic energies of ^{6}He and are shown in Fig. 8c. The ^{4}He, ^{6}He, and ^{7}Li bands, as well as the different low-lying excitation states of ^{209}Bi can be clearly separated. These results further indicate the good performance of both SPA02 and SPA03.

The integrated SPA modules were also applied to the in-beam experiments [29–37] performed at RIBLL1 of IMP. To study the decay properties of the nuclei near the proton drip line, a detector array [32] was composed of three

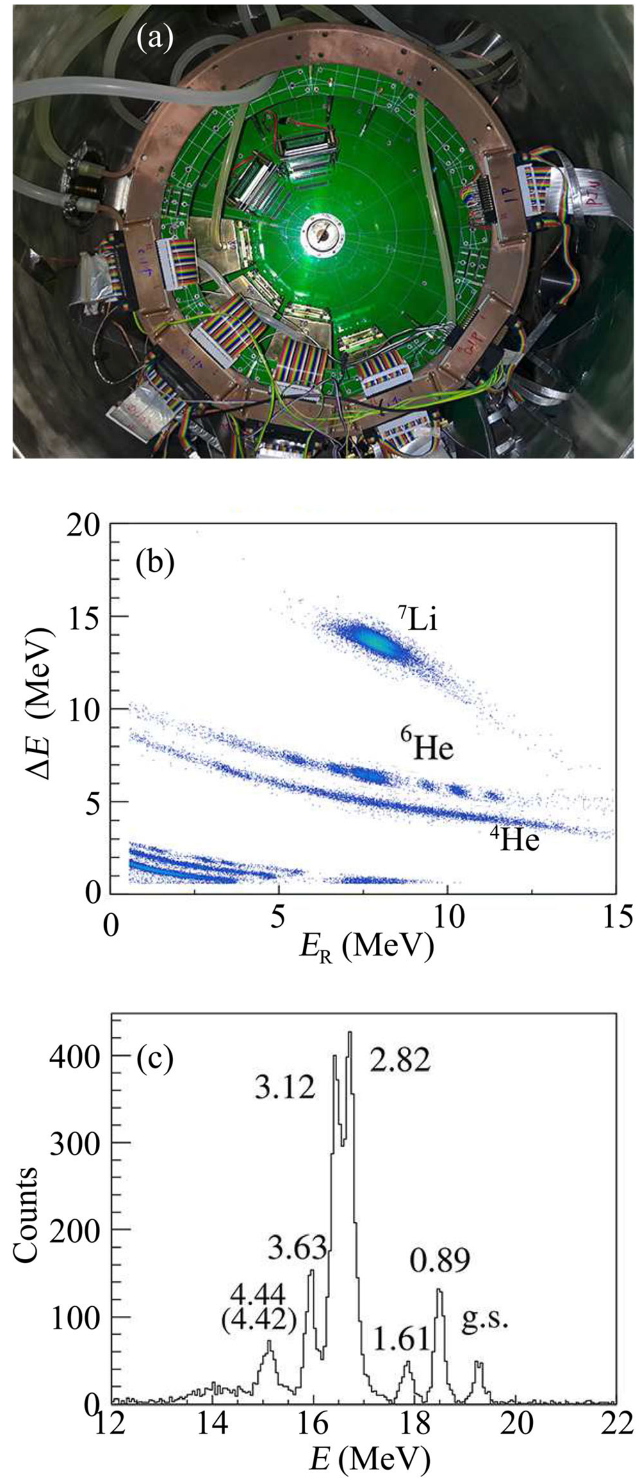

Fig. 8 (Color online) **a** Photograph of the detector array with the SPA02-16 modules and cooling copper ring. **b** ΔE-E_R spectrum obtained by the silicon detector telescope for $^{7}Li+^{208}Pb$ at $E_{lab} = 28.55$ MeV with $\theta_{lab} = 144° - 171°$. **c** The projected energy spectrum of the ^{6}He band where the peaks are labeled corresponding to the excitation states of ^{209}Bi in the unit of MeV

layers of DSSDs with different thicknesses, four 300-μm-thick QSDs, and one 1546-μm-thick QSD. Two SPA03-16 and six SPA02-16 modules were employed to match the 40-μm-thick DSSD and other silicon detectors, respectively.

The photograph of the detector array equipped with the SPA02-16 and SPA03-16 modules for studying the β-decay of ^{27}S is shown in Fig. 9a. Figure 9b shows a typical two-dimensional particle identification spectrum of ΔE-ToF for the secondary beams, where ΔE is given by the QSD with the SPA02 and the ToF is determined by two plastic scintillation detectors located in the RIBLL1 beam-line. The cumulative proton energy spectrum from ^{27}S β-decay measured by the two DSSDs with thicknesses of 40 μm and 304 μm is shown in Fig. 9c. The good quality of the particle identification and the observed proton peaks demonstrate good performance of the SPA02-16 and SPA03-16 modules in the RIB experiment.

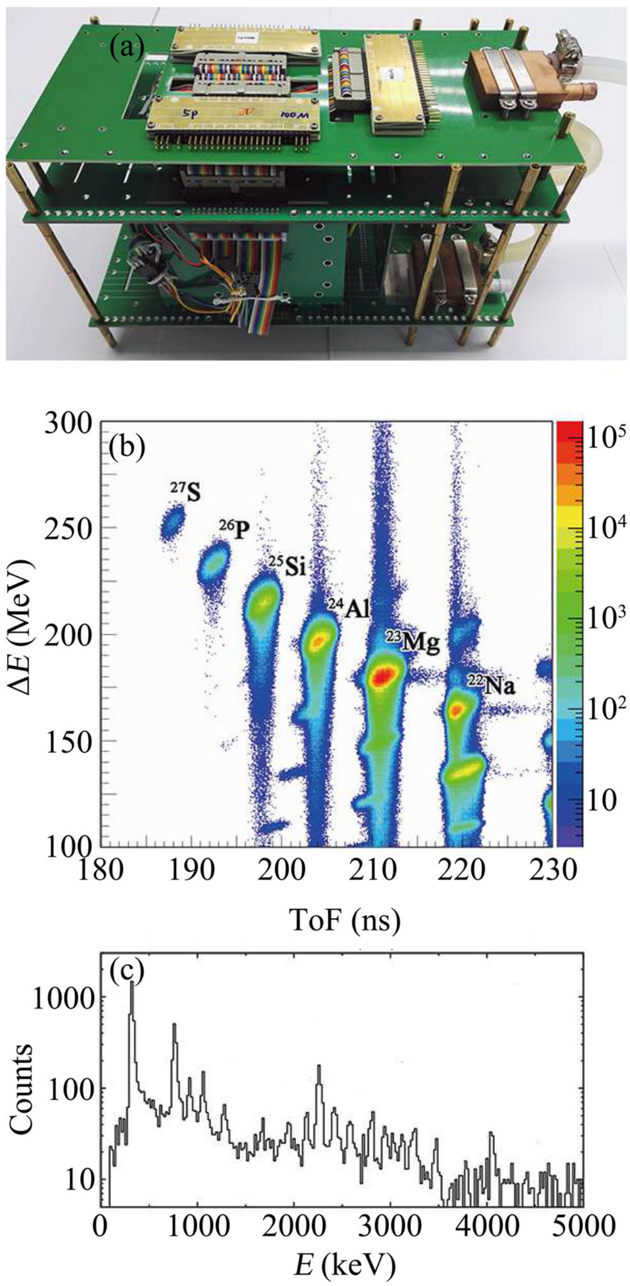

Fig. 9 (Color online) **a** Photograph of the detector array with the modules of SPA02-16 and SPA03-16 equipped with the cooling PCB plate. **b** Typical two-dimensional particle identification spectrum of ΔE-ToF for the secondary beams. **c** Cumulative β-decayed proton energy spectrum for ^{27}S β-decay measured by the 40-μm- and 304-μm-thick DSSDs

4 Summary

In this study, we designed and manufactured two types of integrated charge-sensitive preamplifier modules, namely SPA02-16 and SPA03-16, to match the silicon detector array with a large solid angle coverage, which is widely used in current nuclear experiments. Generally, the SPA02 was produced to support silicon detectors with thicknesses larger than 60 μm, whereas the SPA03 type with external FET was designed to match thin silicon detectors with large parasitic capacitances. The EDR of the SPAs can be easily adjusted by modifying the feedback capacitor C_f for the different experimental requirements.

Both the SPA02 and SPA03 have a fast response and low noise, which is typically less than 6 ns for the rising time and 1.5 keV for the equivalent noise without the external capacitor. The good performance of both SPA02 and SPA03 was further confirmed using an alpha source. A typical energy resolution of 0.6–0.8% was achieved for the silicon strip detectors equipped with the SPAs using the ^{239}Pu alpha source. A maximum EDR of 439 MeV was reached with the C_f of 5 pF. The SPA modules were applied in the in-beam experiments performed at CIAE and IMP; the excellent results further demonstrated the flexibility and stability of the integrated SPA modules.

References

1. I. Tanihata, Nuclear structure studies from reaction induced by radioactive nuclear beams. Prog. Part. Nucl. Phys. **35**, 505 (1995). https://doi.org/10.1016/0146-6410(95)00046-L
2. I. Tanihata, Studies with radioactive beams, past and future. Prog. Theor. Phys. Supp. **146**, 1 (2002). https://doi.org/10.1143/PTPS.146.1
3. T. Motobayashi, Y. Ikeda, K. Ieki et al., Large deformation of the very neutron-rich nucleus ^{32}Mg from intermediate-energy Coulomb excitation. Phys. Lett. B **346**, 9 (1995). https://doi.org/10.1016/0370-2693(95)00012-A
4. Y. Blumenfeld, F. Auger, J.E. Sauvestre et al., MUST: a silicon strip detector array for radioactive beam experiments. Nucl.

Instrum. Methods A **421**, 471 (1999). https://doi.org/10.1016/S0168-9002(98)01178-4
5. E. Pollacco, D. Beaumel, P. Roussel-Chomaz et al., MUST2: A new generation array for direct reaction studies. Eur. Phys. J. A **25**, 287 (2005). https://doi.org/10.1140/epjad/i2005-06-162-5
6. G. Marquínez-Durán, L. Acosta, R. Berjillos et al., GLORIA: a compact detector system for studying heavy ion reactions using radioactive beams. Nucl. Instrum. Methods A **755**, 69 (2014). https://doi.org/10.1016/j.nima.2014.04.002
7. M. Labiche, W.N. Catford, R.C. Lemmon et al., TIARA: a large solid angle silicon array for direct reaction studies with radioactive beams. Nucl. Instrum. Methods A **614**, 439 (2010). https://doi.org/10.1016/j.nima.2010.01.009
8. M. Romoli, M. Di Pietro, E. Vardaci et al., EXODET: a new approach to detection systems for RIB nuclear physics based on ASIC chips developed for high-energy experiments. IEEE Trans. Nucl. Sci. **52**, 1860 (2005). https://doi.org/10.1109/TNS.2005.856890
9. M. Romoli, E. Vardaci, A. Anastasio et al., EXPADES: a new detection system for charged particles in experiments with RIBs. Nucl. Instrum. Methods B **266**, 4637 (2008). https://doi.org/10.1016/j.nimb.2008.05.121
10. N.R. Ma, L. Yang, C.J. Lin et al., MITA: a multilayer ionization-chamber telescope array for low-energy reactions with exotic nuclei. Eur. Phys. J. A **55**, 87 (2019). https://doi.org/10.1140/epja/i2019-12765-7
11. 142A/B/C Preamplifiers. https://www.ortec-online.com/products/electronics/preamplifiers/142a-b-c
12. Mesytec MPR-16-Series. http://www.mesytec.com/products/datasheets/MPR-16.pdf
13. Integrated Circuits Products of IDEAS. https://ideas.no/ideas-ic-products/
14. S. Wang, W. Chen, J.H. Guo, Design and testing of a miniature silicon strip detector. Nucl. Sci. Tech. **31**, 7 (2020). https://doi.org/10.1007/s41365-019-0714-z
15. J.J. Wei, A prototype silicon strip detector for space astronomy. Nucl. Tech. **41**, 120402 (2018). https://doi.org/10.11889/j.0253-3219.2018.hjs.41.120402. (in Chinese)
16. OPA657 1.6 GHz, Low Noise, FET-Input Operational Amplifier. http://www.ti.com/product/OPA657?keyMatch=OPA657&tisearch=Search-EN
17. Micron Semiconductor Ltd. http://www.micronsemiconductor.co.uk/
18. BF862 Datasheet. www.alldatasheet.com/datasheet-pdf/pdf/16238/PHILIPS/BF862.html
19. E. English, A. Weltz, R. Dahal et al., Low-noise preamplifier design considerations for large area high capacitance solid-state neutron detectors. IEEE Trans. Nucl Sci. **63**, 304 (2016). https://doi.org/10.1109/TNS.2016.2516008
20. AD8001 Datasheet. https://www.analog.com/en/products/ad8001.html#product-overview
21. AFG3000C Arbitrary/Function Generator Datasheet. https://www.tek.com/datasheet/afg3000c-arbitrary-function-generator-datasheet
22. N1568A 16Ch Programmable Spectroscopy Amplifier and Dual 16Ch CFD (30% and 80%). https://www.caen.it/products/n1568a/
23. V785 32 Channel Multievent Peak Sensing ADC. https://www.caen.it/products/v785/
24. MSO/DPO4000B Mixed Signal Oscilloscope. https://www.tek.com/oscilloscope/mso4000-dpo4000
25. X.X. Xu, F.C.E. Teh, C.J. Lin et al., Characterization of CIAE developed double-sided silicon strip detector for charged particles. Nucl. Sci. Tech. **29**, 73 (2018). https://doi.org/10.1007/s41365-018-0406-0
26. L. Yang, C.J. Lin, H.M. Jia et al., Abnormal behavior of the optical potential for the halo nuclear system ^{6}He $+^{209}$Bi. Phys. Rev. C **96**, 044615 (2017). https://doi.org/10.1103/PhysRevC.96.044615
27. L. Yang, C.J. Lin, H.M. Jia et al., Optical model potentials for ^{6}He $+^{64}$Zn from ^{63}Cu(^{7}Li,^{6}He)^{64}Zn. Phys. Rev. C **95**, 034616 (2017). https://doi.org/10.1103/PhysRevC.95.034616
28. L. Yang, C.J. Lin, H.M. Jia et al., Is the dispersion relation applicable for exotic nuclear systems? The abnormal threshold anomaly in the ^{6}He $+^{209}$Bi system. Phys. Rev. Lett. **119**, 042503 (2017). https://doi.org/10.1103/PhysRevLett.119.042503
29. L.J. Sun, X.X. Xu, D.Q. Fang et al., β-decay study of the $T_z = -2$ proton rich nucleus ^{20}Mg. Phys. Rev. C **95**, 014314 (2017). https://doi.org/10.1103/PhysRevC.95.014314
30. L.J. Sun, X.X. Xu, C.J. Lin et al., A detection system for charged-particle decay studies with a continuous-implantation method. Nucl. Instrum. Methods A **804**, 1 (2015). https://doi.org/10.1016/j.nima.2015.09.039
31. X.X. Xu, C.J. Lin, H.M. Jia et al., Correlations of two protons emitted from excited states of ^{28}S and ^{27}P. Phys. Lett. B **727**, 126 (2013). https://doi.org/10.1016/j.physletb.2013.10.029
32. X.X. Xu, C.J. Lin, L.J. Sun et al., Observation of β-delayed two-proton emission in the decay of ^{22}Si. Phys. Lett. B **766**, 312 (2013). https://doi.org/10.1016/j.physletb.2017.01.028
33. L.J. Sun, X.X. Xu, C.J. Lin et al., β-decay spectroscopy of ^{27}S. Phys. Rev. C **99**, 064312 (2019). https://doi.org/10.1103/PhysRevC.99.064312
34. L.J. Sun, X.X. Xu, S.Q. Hou et al., Experimentally well-constrained masses of ^{27}P and ^{27}S: implications for studies of explosive binary systems. Phys. Lett. B **802**, 135213 (2020). https://doi.org/10.1016/j.physletb.2020.135213
35. F.F. Duan, Y.Y. Yang, B.T. Hu et al., Silicon detector array for radioactive beam experiments at HIRFL-RIBLL. Nucl. Sci. Tech. **29**, 165 (2018). https://doi.org/10.1007/s41365-018-0499-5
36. Y.T. Wang, D.Q. Fang, X.X. Xu et al., Implantation-decay method to study the β-delayed charged particle decay. Nucl. Sci. Tech. **29**, 98 (2018). https://doi.org/10.1007/s41365-018-0438-5
37. G.L. Zhang, Y.J. Yao, G.X. Zhang et al., A detector setup for the measurement of angular distribution of heavy-ion elastic scattering with low energy on RIBLL. Nucl. Sci. Tech. **28**, 104 (2017). https://doi.org/10.1007/s41365-017-0249-0